Energy Requirements for Ablation or Decomposition of Ceramics During CO_2 and Nd:YAG Laser Machining

Z. Zhang and M. F. Modest
Department of Mechanical Engineering
The Pennsylvania State University
University Park, PA 16802

Abstract

In order to asses *a priori* the outcome of a laser machining process using either simplistic *ad hoc* or sophisticated models, knowledge is needed of the energy required to remove a unit mass of material. Since laser-material interactions involve vaporization, decomposition, ejection of fragments, plasma initiation and expansion, etc., extrapolating enthalpy data from JANAF tables will result in significant uncertainty. In this paper, an experimental setup to measure this "heat of removal" is described.

The apparatus mainly consists of an integrating sphere for the sample and a second integrating sphere for reference. The specimen is mounted at the center of the sample sphere, and is heated by a CO_2 or Nd:YAG laser, whose beam is split, with a part of the beam going into the reference sphere, to monitor the temporal laser power. The energy reflected by the specimen inside the sample sphere is recorded by a second detector. Combining these data, the total absorbed energy may be deduced.

For this type of measurement, energy losses by convection and radiation are generally negligible, while conduction losses may be substantial. In order to minimize conduction losses, the specimens are manufactured to a thickness of less than 500μm. Still, conduction losses may account for up to 10-20 percent of the total laser energy for CW and conventionally pulsed lasers even for such thin samples. Thus, a numerical model is also employed to estimate the conduction losses and to correct the measured value of the "heat of removal."

Experimental data have been obtained for CO_2 and Nd:YAG laser irradiation on graphite, hot-pressed silicon nitride and sintered α-silicon carbide.

Introduction

Extensive application of lasers in materials processing has led to the development of several theoretical models to predict *a priori* the interaction between laser and material, e.g., [1–9]. These range from simple one-dimensional models to complex three-dimensional transient models.

Numerical models as well as simplistic *ad hoc* models are limited in accuracy by the accuracy with which material properties are known. The "heat of removal" as defined here is the laser energy required to remove a unit mass of solid from its substrate by melting/evaporation, by chemical decomposition into gaseous and/or liquid constituents, by micro-explosive removal, etc., depending on the removal mechanism. To our knowledge this quantity has not been measured to date for any material. Presently, the heat of removal has to be estimated by postulating the nature of the removal mechanism, followed by extrapolating enthalpy data from JANAF tables [10], resulting in significant uncertainty in the calculation of material removal rates.

An apparatus has been constructed to measure the heat of removal. The device consists primarily of two integrating-sphere reflectometers. The specimen is mounted inside the sample sphere and is heated by a CO_2 or Nd:YAG laser, a small part of which is split away from the main beam and sent into the reference integrating sphere, which monitors the laser power with an MCT detector. The laser power reflected by the specimen is recorded using a second MCT detector. Integrating the signals from the reflectometers with time allows determination of the laser energy and the energy reflected by the specimen. The laser energy incident on the specimen is dissipated in several ways, namely through reflection, conduction and material removal.

The heat of removal is obtained by subtracting the reflected and conducted components from the incident laser energy.

Conduction losses were estimated using a numerical model previously developed by Modest and co-workers [5–9], which required the experimental determination of the laser intensity profile, the beam size at the focal plane, and the thermophysical properties of the specimen.

A simple device developed by Ramanathan [11] was used to measure the laser intensity profile and laser beam size. Due to the extreme power density of the laser beam at the focal plane, this device can only be used somewhat removed from it. The laser beam diameter at the focal plane can then be calculated from the diameter of the laser beam at several out-of-focus locations.

While thermophysical property data are available in the literature, the data show an order-of-magnitude scatter in diffusivity and conductivity. This scatter in ceramic properties data is probably due to the fact that the properties are significantly affected by porosity and additives. Therefore, to obtain a reasonable estimate for the conduction losses, thermal diffusivity was measured here in a procedure similar to the laser flash method. Since specific heat is a volumetric property, it does not vary as much with impurities and micro-structure as do the thermal diffusivity and conductivity. The specific heat data used here are the same as those of Wallace [12] which were curve-fitted by Ramanathan and Modest [13] and those of Touloukian and Buyco [14].

Three different materials were studied in the present investigation: graphite, hot-pressed silicon nitride and sintered α-silicon carbide. The graphite employed here is black graphite (*McMaster-Carr*). The hot-pressed silicon nitride contains 6wt% Y_2O_3 and 2wt% Al_2O_3 as additives and was purchased from *GTE Inc*. Sintered α-silicon carbide was purchased from *Carborundum Inc.*. No data are available on the additives used in the manufacture of this material. While differences in additives and porosity may have profound influence on the radiative properties and thermal conductivity of a material, these effects are expected to be minor for specific heat and the heat of removal. Experimental results for the heat of removal are presented and compared with values obtained by extrapolation of enthalpy data from the JANAF tables.

Measurements of Laser Beam Profile and Size

The laser beam out of a laser cavity can have different mode structures. For an industrial laser in the moderate to high power range, TEM_{00} and TEM_{01*} tend to be the dominant modes. Assuming a beam of total power P containing only TEM_{00} and TEM_{01*} modes, the intensity distribution can be expressed as [15]:

$$F(r,z) = F_g(z)\left(a + (1-a)\frac{2r^2}{w_g^2(z)}\right)e^{-2r^2/w_g^2(z)}, \tag{1}$$

$$F_g(z) = \frac{2P}{\pi w_g^2(z)}, \tag{2}$$

where $F_g(z)$ is the maximum intensity of a Gaussian TEM_{00} mode laser beam of power P at location z; $w_g(z)$ is the characteristic beam radius; and r is the radial position. The parameter a is the fraction of total intensity that propagates with TEM_{00} mode.

The hyperbolic curve describing the propagation of a laser beam can be expressed as [16]:

$$w_g^2(z) = w_{0,g}^2 + \beta_\infty^2 z^2, \tag{3}$$

where $w_{0,g}$ is the characteristic radius at the focal plane $z = 0$ and β_∞ is the far-field divergence half-angle. The far-field divergence is related to the characteristic radius of the laser waist as:

$$\beta_\infty = \frac{\lambda}{\pi w_{0,g}}, \tag{4}$$

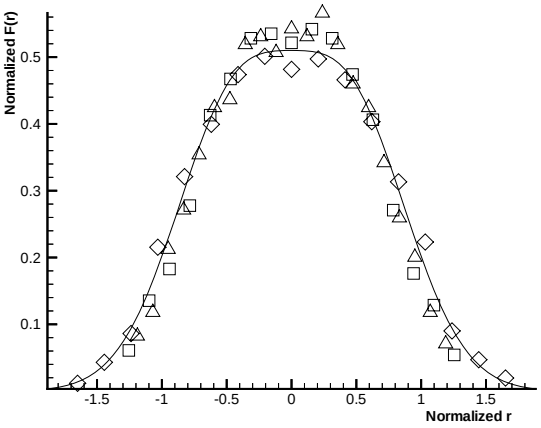

Figure 1: Results of laser beam profile.

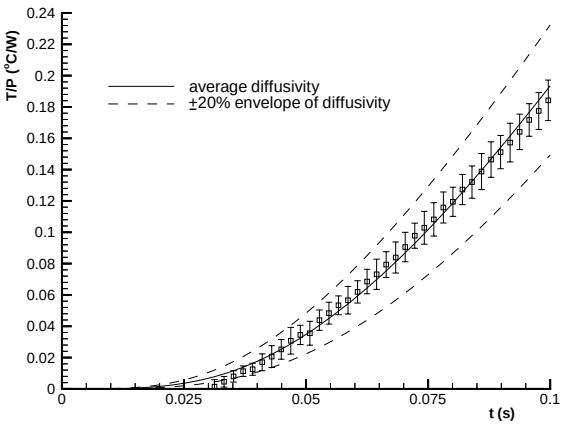

Figure 2: Diffusivity of graphite at room temperature.

where λ is the laser wavelength. Equations (1) through (4) show the characteristic radius at the focal plane $w_{0,g}$ and the fraction of TEM_{00} mode can be deduced by measuring the intensity profile at several z locations.

The simple device used in this study to estimate the spot size and intensity profile of the laser beam, consists of a thermocouple exposed to the laser beam some distance away from the focal plane. It can be readily shown that for a small enough thermocouple the intensity of a laser beam is proportional to the temperature rise of a small thermocouple bead placed in its path [11], and, thus, the temperature rise of the thermocouple bead follows the distribution of the laser beam intensity at location (r, z), where the thermocouple is placed. The measurements were taken with a K-type thermocouple at 95mm, 125mm and 165mm below the focal plane of a 127mm focal length lens with the laser running at 300W. The output of the thermocouple was sent into a digital thermometer (*Omega HH23*). The temperature was taken across the laser beam in 0.5mm steps. The temperature rise was normalized by the maximum temperature rise at the center of a pure TEM_{00} mode beam, and radius r was normalized by the local characteristic radius $w_g(z)$. The resulting non-dimensional values were curve-fitted to the following intensity distribution

$$\overline{F}(\overline{r}) = \left(a + (1-a)2\overline{r}^2\right) e^{-2\overline{r}^2}. \tag{5}$$

The results for a *Coherent Everlase S51* CO_2 laser are shown in Figure 1, which was employed for diffusivity as well as heat of removal measurements. It was found that the characteristic radius of the laser beam at focal plane is $w_{0,g}$ = 125 μm, and the fraction of TEM_{00} mode is 51%. In industry, the radius of a non-Gaussian beam is usually defined as the radius of an aperture through which 86.5% of the total beam power passes. This radius is related to the characteristic radius by a beam quality factor M^2, *i.e.*,

$$w = M w_g. \tag{6}$$

It can be shown that the beam quality factor M^2 for this CO_2 laser is approximately 2.0 [deduced from the value of a in equation (5)] as opposed to the value of 2.7 given by the manufacturer, and the actual beam radius at the focal plane is approximately 175 μm. In a second set of experiments, a *Lumonics JK701* Nd:YAG laser was used, whose beam was delivered through an optical fiber. For this laser the beam radius w_0 was determined to be approximately 420 μm, with a large, unknown M^2 value.

Measurements of Thermal diffusivity

In order to estimate conduction losses during the heat of removal measurements, the thermal diffusivity of the specimen was determined experimentally, for temperatures between room temperature and approximately

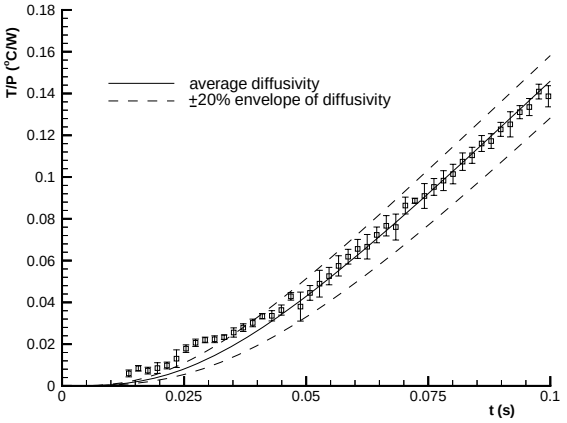

Figure 3: Diffusivity of silicon nitride at room temperature.

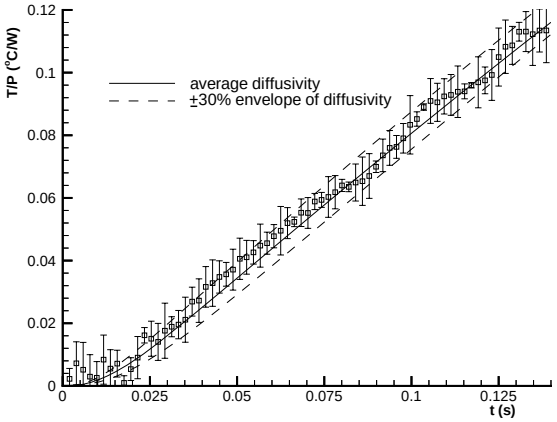

Figure 4: Diffusivity of silicon carbide at room temperature.

1000^{o}C; extrapolation using theoretical predictions was used for temperatures up to the removal point. Since conduction losses during measurements only account for 10$\sim$20% of the total energy, an approximate determination of the temperature-dependent diffusivity to, say, 20% was considered adequate.

The experimental set-up employed here is similar to a laser flash set-up [17]. The front surface of the specimen was subjected to a laser pulse, and a 0.05mm diameter K-type thermocouple bead was pressed against the back surface to measure the back surface temperature at the center of the laser beam. The signal from the thermocouple was sent to a thermocouple amplifier (*Omega OMNI-AMP*), and the output voltage of the amplifier was recorded by a digital oscilloscope (*Nicolet*). The difference between this set-up and a conventional laser flash set-up is that the laser pulse was tuned to a pulse width of 0.5$\sim$1 second. As a result, part of the specimen can reach temperatures of about 1000^{o}C, and the temperature-dependent nature of the thermophysical properties affects the temperature rise at the back surface.

Because the diffusivity is finite, there is a time lag between the beginning of the laser pulse and a significant increase of temperature at the back surface. This results in two distinctive regions in the temperature history at the back surface. The first region has a width of approximately 0.1 second, during which time the temperature rise is relatively slow. The second region corresponds to the time during which the rate of temperature increase is more rapid and relatively uniform over the thickness of the sample. The slope of the temperature history in the second region is governed by the two-dimensional nature of the problem and the non-linearity of the thermophysical properties.

Since the temperature increase in the first region is small, the diffusivity can be treated as constant to deduce the room temperature value. Figures 2 through 4 show the results for graphite, silicon nitride and silicon carbide. The absorptance of materials from previous measurements [18] and measured laser intensity profile were used in deriving the theoretical solutions. It can be seen that the diffusivity uncertainty is well within $\pm$20% for graphite and silicon nitride, as indicated by the dashed lines, while diffusivity uncertainty for silicon carbide is within $\pm$30%.

Once the room temperature diffusivities are known, the diffusivity values at the removal point as used in our model were adjusted to provide a best fit between our theoretical predictions and the experimental results, where it was assumed that thermal conductivity k and specific heat c_p follow trends predicted by quantum mechanics [19], *i.e.*,

$$k(T) = \frac{\delta}{T} + \beta, \tag{7}$$

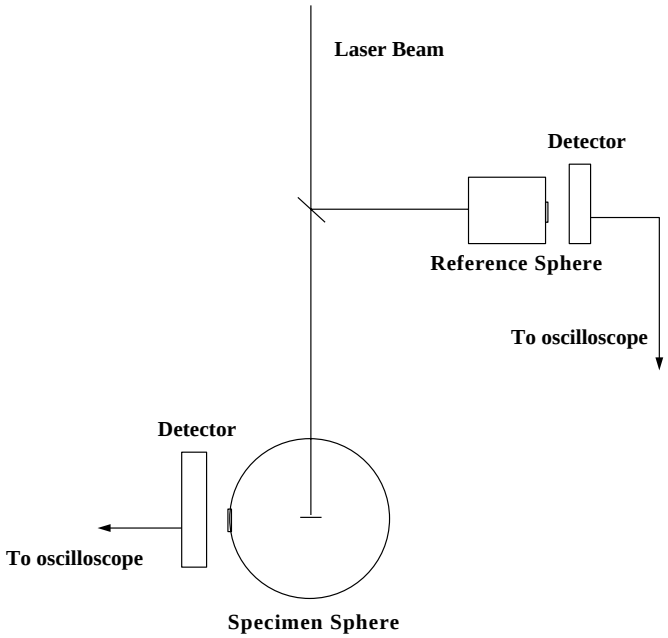

Figure 5: The experimental set-up for heat of removal measurement.

$$c_p(T) = c_{p,\infty}(1 - e^{-T/\gamma}), \tag{8}$$

where $c_{p,\infty}$, δ, β and γ are constants. The density change with temperature was assumed to be negligible, specific heat data were taken from Wallace [12] and Touloukian and Buyco [14], and an iterative procedure was used to determine δ and β from our experiments (including the earlier determination of room temperature diffusivity). It was found that this approach can deduce the diffusivity at the removal point to within $\pm$20%. The results are not suitable to be shown in one simple figure due to the non-linearity of the material properties.

Measurements of the Heat of Removal

Experimental Set-up

The experimental set-up for measurements of the heat of removal is shown in Figure 4. It consists of two integrating spheres, a laser, two detectors, an oscilloscope and optics. The specimen was mounted at the center of the sample integrating sphere (*Labsphere*). The inner wall of the sphere and the sample mount are coated with Infra-Gold, which has a reflectance of 95% over the range of 1$\sim$20μm. The sample sphere is 15cm in diameter, and has a 1.25cm detector port located at its side. The detector port is well baffled from the sample to ensure that the radiation is isotropically scattered before reaching the detector. The specimen was irradiated by a CO_2 laser (*Coherent Everlase S51*) with a 127mm focal length lens in a first set of experiments, while a Nd:YAG laser (*Lumonics JK701*) with a 150mm focal length lens was used in a second set of experiments. The signal was detected by an MCT detector (*Graseby Infrared*). A laserline bandpass filter was put in front of the detector to block the radiation at other wavelengths, thus allowing the measurement of the reflected radiation in the presence of thermal emission from the heated zone. The laser power was monitored by using a beam splitter to redirect a small part of the incident beam into a reference integrating sphere. The signal of the reference sphere was detected by another MCT detector (*Graseby Infrared*). The signals from both integrating spheres were digitally recorded on an oscilloscope (*Nicolet*).

The specimen was then replaced by a standard reference with known reflectance without disturbing the set-up; and the radiation signals from both integrating spheres were recorded. The standard reference used was an Infra-Gold coated sample purchased from *Labsphere*.

Jacquez and Kuppenheim [20] showed that for an integrating sphere with uniform wall coating the radiation, which passes out of an aperture of the sphere, is proportional to the specimen's reflectance and a configuration coefficient. The configuration coefficient is a function of the port area, the inner surface area of the sphere, and the reflectance of the wall coating. When the port area is small compared with the inner surface area of the sphere, which is an appropriate assumption for most integrating spheres, the configuration coefficient can be regarded as a constant. Furthermore, if the detectors are working at their linear range, it follows that

$$V \propto P \propto \rho, \tag{9}$$

where V is the signal from the specimen or reference sphere, P is the power of the radiation, ρ is the reflectance of the laser target. The linearity of the set-up was tested by taking signals under different power levels. It was found the signal was indeed proportional to the radiation power.

The relation between the signal obtained from the reference sphere and the laser power was established by replacing the specimen sphere with a power meter (*Coherent LM5000*). While measuring the laser power, the signal of the reference sphere was also recorded. Since the power meter has a fairly large time constant, it only gives the average laser power, while the reference sphere signal shows the temporal laser intensity. Thus,

$$\overline{P} = c_r \overline{V}_r = \frac{c_r}{t} \int_0^t V_r dt, \tag{10}$$

where $\overline{P}$ is the power meter reading, c_r is the configuration coefficient of the reference integrating sphere, and V_r is the signal from the reference sphere. After determination of c_r the temporal laser power P_l may then be deduced from

$$P_l = c_r V_r. \tag{11}$$

When the laser target is a standard reference, the signal from the specimen sphere is given by

$$V_{st} = c_s \rho_{st} P_l, \tag{12}$$

where c_s is the configuration coefficient of the specimen integrating sphere, and the subscript st refers to "standard reference." Similarly, when the laser target is a specimen, the signal from the specimen sphere is given by

$$V_{sp} = c_s \rho_{sp} P_l, \tag{13}$$

where the subscript sp refers to specimen. Since $\rho_{sp} P_l$ is the power reflected by the specimen, combining Equations (11) through (13), we have

$$\rho_{sp} P_l = \frac{V_{sp}}{c_s} = \frac{V_{sp} \rho_{st} c_r V_r}{V_{st}}. \tag{14}$$

The energy of the incident laser, E_l, and the energy reflected by the specimen, E_ρ, can be expressed as

$$E_l = \int_0^t P_l dt = c_r \int_0^t V_r dt, \tag{15}$$

Run	$E_l - E_\rho$ (J)	m(mg)	E_{cond}(J)	E_{sens}(J)	E_{re}/m(kJ/g)
CO_2:480W	3.81	0.080	0.328	0.667	35.18
CO_2:560W	2.11	0.046	0.163	0.384	33.99
CO_2:560W	4.14	0.092	0.319	0.767	33.19
CO_2:640W	3.56	0.080	0.250	0.667	33.04
CO_2:640W	4.43	0.091	0.311	0.759	36.92
CO_2:665W	4.41	0.101	0.306	0.842	32.29
CO_2:720W	3.28	0.068	0.212	0.567	36.78
Nd:YAG:140W	8.46	0.195	0.327	1.63	33.36
Nd:YAG:140W	8.53	0.187	0.330	1.56	35.50
average E_{re}/m=(34.47$\pm$1.69) kJ/g or $\pm$4.9% experimental uncertainty					

Table 1: Heat of removal for graphite.

$$E_\rho = \int_0^t \rho_{sp} P_l \, dt. \tag{16}$$

Finally, the heat of removal is calculated from

$$E_{\text{re}} = E_l - E_\rho - E_{\text{cond}} - E_{\text{sens}}, \tag{17}$$

where E_{cond} are the conduction losses during the measurement (heating of material that does not become ablated), and E_{sens} is the sensible energy required to raise the temperature of that material to the removal point, which is subsequently ablated.

The mass of ablated material was measured by carefully weighing the specimen before and after each experiment. The weight measurements were done on a *Mettler* micro-balance. It is well known that ablated material can redeposit on the specimen's surface [21], which would affect the accuracy of the measurements. To eliminate such possibility, scanning electronic microscope pictures were taken of each specimen. Examination of the surface surrounding the holes drilled by the laser showed no significant redeposition, probably due to the fact that the depth-to-diameter ratios of these holes are relatively small. The volumes of the holes were also estimated by measuring the top and bottom diameter of the holes, and were found to be within 8% of the weight measurements.

Experimental Results

Between 8 and 9 different measurements were carried out for each material, using two different lasers (*Coherent Everlase S51* and *Lumonics JK701*) and using new specimens for each experiment. Both lasers were running in pulsed mode, with the CO_2 laser running at 250Hz and 2ms on-time/pulse, while the Nd:YAG was laser running at 9.5Hz with 2.5ms on-time/pulse. Each CO_2 experiment was performed at different power levels, to ascertain that there were no serious changes with irradiation levels. However, temporal power densities of the Nd:YAG experiments were roughly identical to the lower CO_2 power levels($\simeq 2 \times 10^6$ W/cm^2 for 480 W), so that overall variation in laser power densities was only about 50%. The conduction losses were estimated separately for each experiment [8]. The energy required to bring a unit mass of the material from room temperature to removal temperature was estimated by integrating the specific heat *vs.* temperature. The values to heat graphite, silicon nitride and silicon carbide were found as 8.34 kJ/g, 2.56 kJ/g and 3.61 kJ/g, respectively, which was used to deduce E_{sens}. Results for each material are given in Tables 1 through 3.

Run	$E_l - E_\rho$ (J)	m(mg)	E_{cond}(J)	E_{sens}(J)	E_{re}/m(kJ/g)
CO_2:560W	3.34	0.198	0.308	0.507	12.75
CO_2:640W	3.47	0.212	0.296	0.543	12.41
CO_2:640W	4.13	0.256	0.352	0.655	12.20
CO_2:640W	4.57	0.296	0.389	0.758	11.56
CO_2:670W	4.09	0.278	0.339	0.712	10.98
CO_2:690W	4.73	0.301	0.385	0.771	11.88
CO_2:720W	3.28	0.213	0.261	0.545	11.61
Nd:YAG:140W	6.60	0.455	0.284	1.16	11.32
Nd:YAG:140W	6.63	0.432	0.285	1.11	12.12
average E_{re}/m=(11.87$\pm$0.56) kJ/g or $\pm$4.7% experimental uncertainty					

Table 2: Heat of removal for silicon nitride.

Run	$E_l - E_\rho$ (J)	m(mg)	E_{cond}(J)	E_{sens}(J)	E_{re}/m(kJ/g)
CO_2:480W	2.61	0.139	0.321	0.502	12.86
CO_2:560W	2.87	0.160	0.290	0.578	12.51
CO_2:640W	2.95	0.164	0.276	0.592	12.70
CO_2:640W	3.02	0.183	0.282	0.661	11.35
CO_2:720W	2.14	0.125	0.186	0.451	12.02
CO_2:720W	1.79	0.093	0.155	0.336	13.97
Nd:YAG:140W	5.86	0.364	0.342	1.31	11.55
Nd:YAG:140W	5.07	0.301	0.296	1.09	12.25
average E_{re}/m=(12.40$\pm$0.83) kJ/g or $\pm$6.7% experimental uncertainty					

Table 3: Heat of removal for silicon carbide.

Note that results for CO_2 and Nd:YAG laser irradiation are virtually identical, showing that the heat of removal is independent of wavelength and that uncertainty due to variable absorptance (temperature and wavelength dependence) is negligible. However, both lasers employed here have fairly similar pulse duration and powers. It is quite likely that laser irradiation with much higher powers/shorter pulses would result in slightly higher removal temperature and slightly different heat of removal. While the tables show less than 7% of uncertainty, the overall uncertainty is somewhat larger due to systematic errors inherent to the present experimental scheme. As mentioned earlier, our diffusivity estimation can predict the thermal diffusivity of the materials at room temperature to within 30%, and predict that at the removal temperature to within 20%. Calculations with our numerical model show that for our heat of removal measurements, the uncertainty of the thermal diffusivity of the materials can cause up to $\pm$10% systematic error in the estimated conduction loss. Similarly, the estimation of E_{sens} from specific heat data and assumed removal temperature will also result in a systematic error in the the heat of removal. Including these errors, we estimate the overall uncertainty for the heat of removal values to be within $\pm$10%.

According to the JANAF tables, graphite is expected to decompose into almost pure C_3 at an ablation temperature of approximately 4000K [10]. Based on this, Modest et al. [27] have estimated the heat of removal for graphite to be approximately 20 kJ/g. The experimental results show that the heat of removal of graphite is considerably larger than 20 kJ/g, suggesting that the decomposition products consist to a large part of gaseous C_2 and possibly some C_1 and C_3.

The decomposition reaction of crystalline silicon nitride is well known to be [22]

$$Si_3N_4(s) \rightarrow 3Si(l) + 2N_2(g). \tag{18}$$

Based on a decomposition temperature of approximately 2151K [23], Roy and Modest [6] have calculated the heat of removal for silicon nitride, using the absolute enthalpies values from the JANAF tables, as 6.2 kJ/g. The maximum possible heat of removal for silicon nitride, according to the JANAF tables, is 14.2 kJ/g, *i.e.*, if silicon is leaving as a gas rather than a liquid. The experimental result is somewhat below this maximum, suggesting that a substantial amount of liquid silicon is evaporated before leaving the ablation zone.

While silicon carbide is known to decompose into a number of gaseous products upon heating, various investigations have led to conflicting results [24–26]. Ramanathan [11] estimated the heat of removal for silicon carbide from the JANAF tables as 12.1 kJ/g, by postulating the nature of the decomposition mechanism. His results agree well with our experimental results.

Conclusions

The energy requirements to remove a unit mass of material by a CO_2 or Nd:YAG laser ("heat of removal") during laser materials processing has been measured for several important industrial ceramics. The experimental apparatus incorporates two integrating spheres, and measures the temporal power and power reflected by the specimen simultaneously. A numerical model was used to estimate conduction losses. The experimental results have been presented with an overall uncertainty of approximately $\pm 10\%$. It was found that the heat of removal is insensitive to the laser wavelength, as well as to laser power (at least over the peak power levels between 2.0×10^6 W/cm^2 and 3.0×10^6 W/cm^2 at the beam center, as were used in the present experiments). Comparison with "most likely" values calculated from the JANAF tables showed that such values can be seriously in error.

Acknowledgment

Support for this work by the National Science Foundation through Grant CTS-9312325 is gratefully acknowledged.

References

1. Dabby, F. W., and U.-C. Paek (1972), High-Intensity Laser-Induced Vaporization and Explosion of Solid Material, **IEEE J. Quantum Electron. QE-8**, 106–111.
2. Abakians, H., and M. F. Modest (1988), Evaporative Cutting of a Semi-Transparent Body with a Moving CW Laser, **J. Heat Transfer 110**, 924–930.
3. Chryssolouris, G. (1991), Laser Machining: Theory and Practice, Springer Verlag, New York, NY.
4. Vorreiter, J. O., D. A. Kaminski, and R. N. Smith (1991), MonteCarlo Simulation of a Laser Drilling Process, ASME paper no. 91-WA-HT-9.
5. Ramanathan, S., and M. F. Modest (1992), CW Laser Drilling of Composite Ceramics, In *Proceedings of ICALEO '91, Laser Materials Processing*, Vol. 74, 305–326, San Jose, CA.
6. Roy, S., and M. F. Modest (1993), CW Laser Machining of Hard Ceramics — Part I: Effects of Three-Dimensional Conduction and Variable Properties and Various Laser Parameters, **Int. J. Heat Mass Transfer 36**(14), 3515–3528.
7. Bang, S. Y., S. Roy, and M. F. Modest (1993), CW Laser Machining of Hard Ceramics — Part II: Effects of Multiple Reflections, **Int. J. Heat Mass Transfer 36**(14), 3529–3540.
8. Modest, M. F. (1996), Three-Dimensional, Transient Model for Laser Machining of Ablating/Decomposing Materials, **Int. J. Heat Mass Transfer 39**(2), 221–234.
9. Modest, M. F., S. Ramanathan, A. Raiber, and B. Angstenberger (December 1995), Laser Machining of Ablating Materials–Overlapped Grooves and Entrance/Exit Effects, **J. Laser Appl. 7**(4), 210–218.

10. Chase, J. M. W., C. A. Davies, J. J. R. Downey, D. J. Frurip, R. A. McDonald, and A. N. Syverud (Editors) (1985), JANAF Thermochemical Tables, National Bureau of Standards, Washington, DC.

11. Ramanathan, S. (1993), Laser Cutting and Drilling of Ceramics and Ceramic Composites, PhD thesis, The Pennsylvania State University, University Park, PA.

12. Wallace, R. J. (1983), A Study of the Shaping of Hot Pressed Silicon Nitride With a High Power *CO_2 Laser*, PhD thesis, University of Southern California, Los Angeles, CA.

13. Ramanathan, S., and M. F. Modest (1990), Effects of Variable Thermal Properties on Evaporative Cutting with a Moving CW Laser, In *Heat Transfer in Space Systems*, Vol. HTD–135, 101–108, ASME.

14. Touloukian, Y. S., and E. H. Buyco (Editors) (1970), Specific Heat: Nonmetallic Solids Vol. 5 of *Thermophysical Properties of Matter*, Plenum Press, New York.

15. Philips, R. L., and C. L. Andrews (1986), Spot size and divergence for Laguerre Gaussian Beams of any order, **J. Heat Transfer 108**, 597–601.

16. Kogelnik, H., and T. Li (1956), Laser Beams and Resonators, **Appl. Opt. 5**(10), 1550–1565.

17. Parker, W. J., R. J. Jenkins, C. P. Butler, and G. L. Abbott (19719616), Flash Method of Determining Thermal Diffusivity, Heat Capacity, and Thermal Conductivity, **Journal of Applied Physics 32**, 1216793–1684.

18. Zhang, Z., and M. F. Modest (1996), Temperature-Dependent Absorptances of Ceramics for Nd:YAG and CO_2 Laser Processing Applications, In *Proceedings of the Materials Processing Cutting Symposium ICALEO '96, Detroit, MI*, Vol. 81C, 29–38.

19. Tien, C. L., and J. H. Lienhard (1971), Statistical Thermodynamics, Holt, Rinehart & Winston, New York.

20. Jacquez, J. A., and H. F. Kuppenheim (1955), Theory of the Integrating Sphere, **J. Opt. Soc. Am. 45**, 460–470.

21. DeBastiani, D., M. F. Modest, and V. S. Stubican (1990), Mechanisms of Reactions During *CO_2*-Laser Processing of Silicon Carbide, **J. Amer. Cer. Soc. 73**(7), 1947–1952.

22. Singhal, S. C. (1976), Thermodynamic Analysis of the High Temperature Stability of Silicon Nitride and Silicon Carbide, **Ceramurgia Int. 2**, 123–130.

23. Pehlke, R. D., and J. F. Elliott (1959), High-Temperature Thermodynamics of the Silicon, Nitrogen, Silicon-Nitride System, **Transactions of the Metallurgical Society of AIME 215**, 781–785.

24. Drowart, J., G. De Maria, and M. G. Inghram (1958), Thermodynamic Study of SiC Utilizing a Mass Spectrometer, **Journal of Chemical Physics 29**, 1015–1021.

25. Scace, R. I., and G. A. Slack (1960), The Si-C and Ge-C Phase Diagrams, Silicon Carbide, Pergamon Press.

26. Baird, J. D., and A. Taylor (1958), Reaction Between Silica and Carbon and the activity of Silica in Slag Solution, **Transactions of the Faraday Society 54**, 526–539.

27. Modest, M. F., S. Ramanathan, A. Raiber, and B. Angstenberger (1994), Laser Machining of Ablating Materials–Overlapped Grooves and Entrance/Exit Effects, In *Proceedings of ICALEO '94*, 303–312.

Meet the Authors

Zhaoyan Zhang is a doctoral graduate student in mechanical engineering at the Pennsylvania State University. Before coming to the U.S. he obtained his bachelor's and master's degrees in P. R. China in 1990 and 1995, respectively. Currently, he is doing research on radiative properties measurements relevant to laser materials processing.

Michael F. Modest was born in Germany and received his Dipl.-Ing. degree in Mechanical Engineering from the Technical University in Munich in 1968. After coming to the U.S. he obtained his M.S. and Ph.D. degrees, also in Mechanical Engineering, from the University of California at Berkeley in 1972. He is presently a professor in the Mechanical Engineering Department at the Pennsylvania State University. His research interests cover two major areas in experiment as well as in theory: radiative heat transfer, and heat transfer during laser machining of ceramics.